ISSN 1990-7931, Russian Journal of Physical Chemistry B, 2017, Vol. 11, No. 2, pp. 261–271. © Pleiades Publishing, Ltd., 2017.
Original Russian Text © K.A. Avdeev, V.S. Aksenov, A.A. Borisov, D.G. Sevastopoleva, R.R. Tukhvatullina, S.M. Frolov, F.S. Frolov, I.O. Shamshin, B. Basara, W. Edelbauer, K. Pachler, 2017, published in Khimicheskaya Fizika, 2017, Vol. 36, No. 4, pp. 20–31.

COMBUSTION, EXPLOSION, AND SHOCK WAVES

Calculation of Shock Wave Propagation in Water Containing Reactive Gas Bubbles

K. A. Avdeev[a, b], V. S. Aksenov[a, b, c], A. A. Borisov[a, b], D. G. Sevastopoleva[b, c], R. R. Tukhvatullina[a], S. M. Frolov[a, b, c, *], F. S. Frolov[a, b], I. O. Shamshin[a, b, c], B. Basara[d], W. Edelbauer[d], and K. Pachler[d]

[a] *Semenov Institute of Chemical Physics, Russian Academy of Sciences, Moscow, 119991 Russia*
[b] *Center of Pulse Detonation Combustion, Moscow, 119991 Russia*
[c] *National Research Nuclear University MEPhI, Moscow, 115409 Russia*
[d] *AVL List GmbH, 8020 Graz, Austria*
**e-mail: smfrol@chph.ras.ru*

Received August 29, 2016

Abstract—The entry of a shock wave from air into water containing reactive gas (stoichiometric acetylene–oxygen mixture) bubbles uniformly distributed over the volume of the liquid has been numerically investigated using equations describing two-phase compressible viscous reactive flow. It has been demonstrated that a steady-state supersonic self-sustaining reaction front with rapid and complete fuel burnout in the leading shock wave can propagate in this bubbly medium. This reaction front can be treated as a detonation-like front or "bubble detonation." The calculated and measured velocities of the bubble detonation wave have been compared at initial gas volume fraction of 2 to 6%. The observed and calculated data are in satisfactory qualitative and quantitative agreement. The structure of the bubble detonation wave has been numerically studied. In this wave, the gas volume fraction behind the leading front is approximately 3–4 times higher than in the pressure wave that propagates in water with air bubbles when the other initial conditions are the same. The bubble detonation wave can form after the penetration of the shock wave to a small depth (~300 mm) into the column of the bubbly medium. The model suggested here can be used to find optimum conditions for maximizing the efficiency of momentum transfer from the pressure wave to the bubbly medium in promising hydrojet pulse detonation engines.

Keywords: bubbly medium, reactive gas, shock wave, hydro-shock tube, reacting two-phase flow
DOI: 10.1134/S1990793117020142

INTRODUCTION

In our patent [1] and articles [2–4], we suggest that hydrojet thrust can be created using a hydrojet pulse detonation engine instead of a mechanical propulsion device like a propeller, impeller, or another type. The principal elements of the hydrojet pulse detonation engine are a pulse detonation tube periodically filled with a fuel–air mixture for generating a shock wave (SW) and a shaped water conduit in which outboard water is accelerated by the SW to produce hydrojet thrust. For efficiently involving outboard water in motion behind the SW, it is suggested [1] to increase the compressibility of water in the conduit by sparging it with a chemically inert or reactive gas. In our earlier publications [2–4], we reported experimental and calculated data concerning pulse momentum transfer from the SW to water containing air (chemically inert gas) bubbles.

The entry of an SW into a liquid with reactive gas bubbles uniformly distributed over its volume can give rise to "bubble detonation," which is a self-sustaining detonation-like pressure wave propagating quasi-steadily at a supersonic speed [5–9]. Apparently, bubble detonation was observed for the first time in a vertical tube with a square cross section (50 × 50 mm) and a length of 1985 mm [5]. The purpose of those experiments was to investigate SW propagation through a column of liquid glycerol containing a chain of bubbles of a reactive gas (30% ($2H_2 + O_2$) + 70% Ar). The chain length was ~670 mm, and the average bubble diameter was ~10 mm. Later, Sychev et al. [6–8] carried out systematic experimental studies of bubble detonation in the liquid (water) with reactive gas (stoichiometric acetylene–oxygen mixture) bubbles in a vertical hydro-shock tube with an inner diameter of 35 mm and a total height of 5635 mm with a bubbly medium column height of 4195 mm. In the experiments reported in Refs. [7, 8], bubble detonation was initiated by admitting gas detonation into a column of a bubbly medium with an initial gas volume fraction

(α_{20}) of up to 8–10%. In those experiments, bubble detonation arose only at relatively small α_{20} values not exceeding 6% (upper gas concentration limit) at a fairly long distance from the gas/bubbly medium interface (2.5–3.5 m). Attempts to initiate bubble detonation in water containing more gas were unsuccessful. At gas volume fractions below 0.5% (lower gas concentration limit), bubble detonation was not observed either.

There has been a series of experiments concerning the liquid viscosity effect on the initial gas volume fraction limits within which bubble detonation can take place [9]. Those experiments were carried out under conditions similar to those specified in Refs. [7, 8]. It was found that increasing the viscosity of the liquid (by adding up to 50 vol % glycerol to water) makes it possible to initiate bubble detonation at a lower amplitude of the initiating SW (17 atm against 40–50 atm in Refs. [7, 8]). It was also observed that the viscosity of the liquid has an effect on the initial gas concentration limits of detonation. The initiation of bubble detonation in water containing up to 25 vol % glycerol by an SW with amplitude of 17 atm was possible only at an initial gas volume fraction of 1%. Increasing the initial gas volume fraction to 6% necessitated that the SW amplitude be raised to 60 atm.

The main specific features of bubble detonation were reported in earlier works [5–9]. Firstly, the bubble detonation velocity is always higher than the SW velocity in the same liquid with chemically inert gas bubbles under similar conditions and is certainly higher than the speed of sound in the bubbly medium. For example, at $\alpha_{20} \approx 2\%$ the bubble detonation velocity is ~560 m/s, the SW velocity is ~425 m/s, and the low-frequency sound speed is ~85 m/s [7]. Secondly, the propagation of bubble detonation is a self-sustaining process [7], while an SW in a liquid containing chemically inert gas bubbles gradually decays.

For employing bubble detonation in hydrojet pulse detonation engines, for example, for producing thrust, it is necessary to know whether it is possible to initiate detonation or a detonation-like regime in water at short distances (below 1 m) in a wide range of gas volume fractions. This information can be gained, for example, by constructing a physical and mathematical model of the process and by performing the corresponding numerical calculations. In addition, these calculations would make it possible to determine the parametric region of existence of bubble detonation.

The existing one-dimensional (1D) physico–mathematical models of the process [10–12] are based on the assumption that the velocities of the phases in the medium are equal. A 1D two-velocity single-temperature model was suggested [13] for describing the bubble detonation wave structure. We proposed [2–4] a multidimensional, two-temperature, two-velocity, two-phase, nonreacting flow model, and this model was used to calculate the SW propagation velocity in water with air bubbles. In this work, we extend the previous model [2–4] to liquid flows containing reactive gas bubbles and validate the new model against experimental data.

MATHEMATICAL MODEL

The mathematical model of two-phase, compressible, viscous, reactive flow is based on the system of differential equations of mass, momentum, and energy conservation that was used in our earlier studies [2–4]. In this work, as distinct from those earlier studies [2–4], in which bubbles of a chemically inert gas (air) were considered, the system of determining equations is supplemented with chemical source terms in the continuity equation for the ith chemical species, $\alpha_2\dot{\omega}_i$, and in the energy conservation equation for the gas phase, $\alpha_2\dot{\omega}_T$, where α_2 is the gas volume fraction in the bubbly medium. The form of these source terms will be discussed below.

Since one of the main objects of experimental studies by Sychev et al. [6–9] was water containing bubbles of a stoichiometric acetylene–oxygen mixture, to simplify the pronlem it was assumed that the following irreversible one-step reaction can occur in the bubbles:

$$C_2H_2 + 2.5O_2 \rightarrow 2CO_2 + H_2O. \quad (1)$$

According to the phenomenological law of chemical kinetics, the source term $\dot{\omega}_i$ is expressed as

$$\dot{\omega}_i = W_i(\nu_i'' - \nu_i')Ae^{-E/RT_2}\left(\frac{Y_F\rho_2}{W_F}\right)\left(\frac{Y_{Ox}\rho_2}{W_{Ox}}\right) \quad (2)$$

with an overall preexponential factor of $A = 2\times 10^8$ m^3/(kmol s) and an overall activation energy of $E = 47409$ J/mol in the expression for the rate constant of the bimolecular reaction [14]; here, ν_i' is the stoichiometric coefficient of species i that is a reactant, ν_i'' is the stoichiometric coefficient of species i that is a reaction product, R is the universal gas constant, W_i is the molar mass of species i, Y_i is the weight fraction of species i, and the subscripts F and Ox stand for acetylene and oxygen, respectively.

For the source term in the energy conservation equation, $\alpha_2\dot{\omega}_T$, we have

$$\alpha_2\dot{\omega}_T = -\alpha_2\rho_2\sum_i\left(\Delta h_{f,i}^0\right)\frac{dY_i}{dt}, \quad (3)$$

where $\Delta h_{f,i}^0$ is the enthalpy of formation of the ith species of the gas phase. Note that the model allows use of detailed kinetic mechnisms of fuel oxidation, however, at this stage of our study, use of such mechanisms would be premature.

ALGORITHM

The system of governing equations [3] was represented as a generalized equation for the variable $\phi_k(x, t)$, where the subscript k designates a certain phase (1—liquid, 2—gas):

$$\underbrace{\frac{\partial \alpha_k \rho_k \phi_k}{\partial t}}_{\text{Rate of variation, } R} + \underbrace{\nabla \alpha_k \rho_k \mathbf{v}_k \phi_k}_{\text{Convection, } C} - \underbrace{\nabla \alpha_k \Gamma_{\phi k} \nabla \phi_k}_{\text{Diffusion, } D} = \underbrace{\nabla \alpha_k \mathbf{S}^A_{\phi k} + S^V_{\phi k}}_{\text{Sources, } S}. \quad (4)$$

On the left-hand side of Eq. (4), the first term (R) accounts for the time variation of the variable ϕ_k; the second term (C), for convective transport; the third term (D), for transport due to diffusion ($\Gamma_{\phi k}$ is the diffusion coefficient). On the right-hand side of Eq. (4), the term S stands for the source terms ϕ_k, which include the bulk sources, $S^V_{\phi k}$, and the surface sources, $\nabla \alpha_k \mathbf{S}^A_{\phi k}$. (They include the part of the diffusion flux that is not taken into account in the term D.)

By intergrating Eq. (4) over some polyhedral cell P and applying the Gauss–Ostrogradsky theorem, we obtain

$$\underbrace{\frac{d}{dt}\left(\alpha_k \rho_k \varphi_k \ V_{\text{cel}}\right)_P}_{R} + \sum_{f=1}^{n_f} \underbrace{\left(\alpha_k \rho_k \mathbf{v}_k \mathbf{A} \phi_k\right)_f}_{C_f} - \sum_{f=1}^{n_f} \underbrace{\left(\alpha_k \Gamma_{\phi k} \nabla \varphi_k \mathbf{A}\right)_f}_{D_f} = \sum_{f=1}^{n_f} \underbrace{\left(\alpha_k \mathbf{S}^A_{\phi k} \mathbf{A}\right)_f}_{S^A_\phi} + \underbrace{\left(S^V_{\phi k} V_{\text{cel}}\right)_P}_{S^V_\phi}, \quad (5)$$

where the subscript P is given to the values of variables at the center of the cell, the subscript f is given to the values of variables at the center of a face, the terms C_f and D_f account for convective and diffusion transport of the variable ϕ_k through face f, n_f is the number of faces in the cell P, $\mathbf{A}_f$ is the area of face f, and V_{cel} is the volume of the cell. All dependent variables (volume fraction, density, velocity, pressure, enthalpy, and species concentrations) are defined at the centers of the cells. The system of equations (5) was solved using the segregated algorithm SIMPLE [15, 16]. Convective transport in the mass conservation law was approximated using a central difference; in the momentum conservation law, it was approximated using the TVD scheme with the MINMOD limiter [17]; for the other equations, we used the standard first-order UPWIND scheme.

The chemical source terms were calculated for a fixed volume using the implicit second-order Adams method with an internal integration step. The system of determining equations was numerically integrated using the solver of the AVL FIRE® computational package.

CALCULATED DATA

Velocity of Pressure Waves in the Bubbly Medium under Experimental Conditions Specified in Ref. [7]

In order to verify the model developed, we carried out calculations for conditions similar to the experimental conditions specified in Ref. [7]. The calculations were performed in the 1D approximation retaining the main geometric parameters of the hydro-shock tube [7]. Velocity slip and zero heat flux conditions were imposed on the tube wall. The calculations were carried out using various computational grids until obtaining grid-independent results such that further grid refinement and diminishing the step of integration with respect to time had no effect on the pressure wave velocity in the bubbly medium.

The experiments reported in Ref. [7] were performed in a vertical hydro-shock tube (Fig. 1a) with an inner diameter of 35 mm. The high initial pressure in the high-pressure chammber (HPC) was generated [7] by burning the stoichiometric acetylene–oxygen mixture . The low-pressure chamber (LPC) was filled with air at atmospheric pressure. A water column with an initial gas volume fraction of $\alpha_{20} = 1–10\%$ was created in the measurement section (MS). The average size of the reactive gas (stoichiometric acetylene–oxygen mixture) bubbles was $d_{20} = 3.5–4.0$ mm. The water, air, and reactive gas in the experiments [7] were at room temperature. The experimental values of the average velocity of the pressure waves under these conditions are presented in Fig. 1b. The velocity values were derived from pressure data recorded with the sensors P5 and P6 (Fig. 1a). Note that bubble detonation in those experiments [7], in which acetylene combustion products emitted light, was observed at $\alpha_{20} = 2$ to 6% (black squares), while no light emission from acetylene combustion products was detected at $\alpha_{20} > 6\%$, whence it was inferred [7] that there was no detonation (open squares).

The calculations were carried out for the following conditions. Parameters of the medium in the HPC (1150 mm in length): air at an initial pressure of 6.3 MPa and an initial temperature of 4278 K; i.e., the acetylene–oxygen mixture combustion products were replaced by air with the corresponding initial parameters calculated using a thermodynamic code. Parameters of the medium in the LPC (290 mm in length): air at an initial pressure of 0.1 MPa and an intial temperature of 293 K. Parameters of the medium in the MS (4195 mm in length): water with bubbles of the stoichiometrc acetylene–oxygen gas mixture (C_2H_2 and O_2 mass fractions of 0.2453 and 0.7547, respectively) at an initial pressure of 0.1 MPa and an initial temperature of 293 K.

The solid and dashed curves in Fig. 1b represent the numerically calculated dependences of the pressure wave velocity on the gas volume fraction in water.

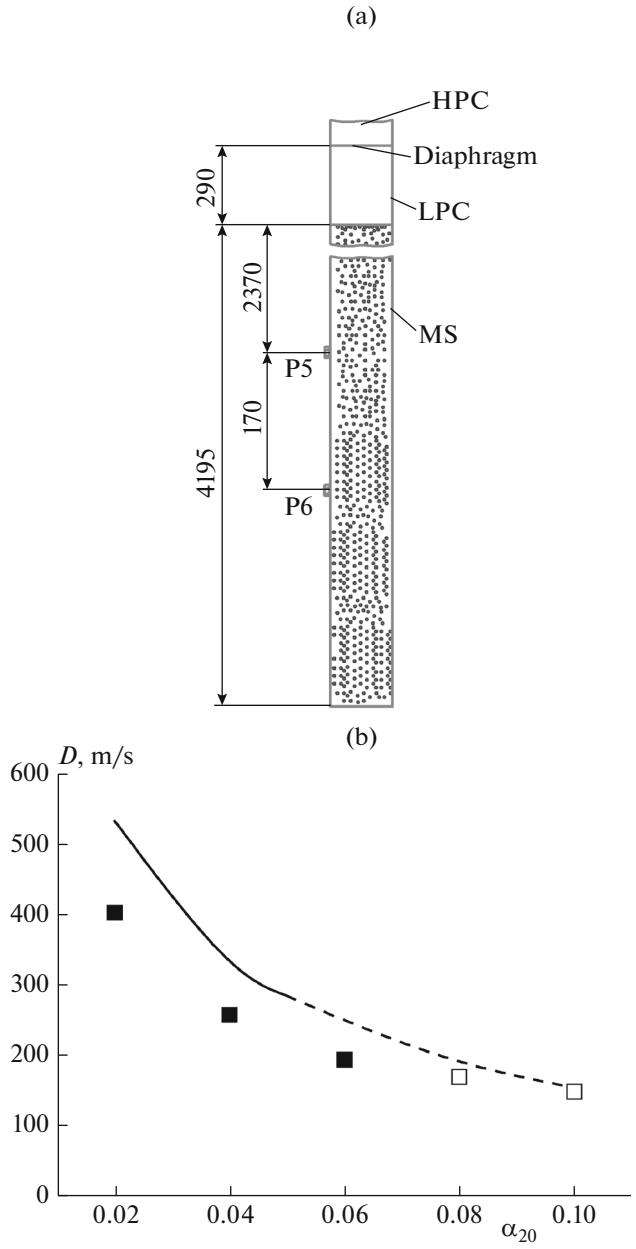

Fig. 1. Comparison of the results of the calculations with experimental data from Ref. [7]: (a) experimental setup (dimensions in millimeters); (b) calculated (curve) and measured (squares) pressure wave velocities as a function of the initial gas volume fraction in water containing acetylene–oxygen mixture bubbles.

The velocity of the pressure wave was determined 2370 mm away from the air/bubbly medium interface (coordinate of the pressure sensor P5 in Fig. 1a). In the calculations for α_{20} = 2–5%, the velocity of the pressure wave did not vary along the bubbly medium column, so such waves were treated as waves of self-sustaining bubble detonation. Clearly, although the calculated bubble detonation velocity (solid curve) is higher than the velocity measured at α_{20} = 2–6% [7], it decreases with an increasing α_{20}, just as is observed in the experiment. The calculated upper gas concentration limit of bubble detonation (5%) is slightly lower than the experimental limit (6%). At $\alpha_{20} > 5\%$, the calculated pressure waves decay along the bubbly medium column; for this reason, these waves are not assigned to self-sustaining bubble detonation waves (dashed curve). It can be seen in Fig. 1b that, in this range of gas volume fraction, the calculated and experimental data are in much better agreement. The structure of both types of waves will be discussed in the next subsection.

Note that, at all gas volume fractions, both the measured and calculated pressure wave velocities are higher than the maximum (low-frequency) speed of sound in water containing gas bubbles. The low-frequency speed of sound, c_0, is given by the following formula [18]:

$$c_0^2 = \frac{1}{\alpha_{10}\rho_{10} + \alpha_{20}\rho_{20}}\left(\frac{\alpha_{10}}{c_{10}^2\rho_{10}} + \frac{\alpha_{20}}{c_{20}^2\rho_{20}}\right)^{-1}. \qquad (6)$$

Under the conditions of the experiments carried out by Sychev [7], the low-frequency speed of sound was approximately 85 m/s at α_{20} = 2% and 40 m/s at α_{20} = 10%; that is, the pressure waves under these conditions propagated at a Mach number of $M = D/c_0 = 5$ and 3.7, respectively. In other words, the pressure waves depicted in Fig. 1b are essentially supersonic.

Velocity and Structure of Pressure Waves in the Bubbly Medium in the Hydro-Shock Tube [4]

To understand the properties of the supersonic pressure waves, first of all it is necessary to consider their spatial structure obtained by numerical calculations. The calculations were carried out for a vertical hydro-shock tube with a 50 × 100 mm rectangular cross section [4]. Initially, we investigated SW propagation in water with air bubbles; next, we studied the same process in water containing reactive gas bubbles. The calculations were performed in the two-dimensional approximation in which all basic geometyric parameters of the shock tube [4] were retained. Velocity slip and zero heat flux conditoions were imposed on the tube wall.

Figure 2a shows one of the hydro-shock tube configurations used in the experimental studies of bubble detonation in water with bubbles of the stoichiometric acetylene–oxygen mixture. The high pressure (~6.3 MPa) in the HPC of this tube was created by burning the stoichiometric propane–oxygen mixture. The LPC was filled with air at atmospheric pressure. A water column with an initial gas volume fraction of α_{20} = 2 to 30% was produced in the MS. The size of

the reactive gas bubbles in this section was d_{20} = 1.5–4 mm. All media in the experiments were initially at room temperature. A transparent optical sdection was built in the MS for high-speed video recording of the process.

The calculations were carried out for the following conditions. Parameters of the medium in the HPC (495 mm in length): air at an initial pressure of 6.3 MPa and an intial temperature of 3860 K; i.e., the propane–oxygen mixture combustion products were replaced by air with initial parameters close to those calculated using a thermodynamic code. Parameters of the medium in the LPC (70 mm in length): air at an initial pressure of 0.1 MPa and an initial temperature of 293 K. Parameters of the medium in the MS (920 mm in length): water with bubbles of the stoichiometric acetylene–oxygen gas mixture at an initial pressure of 0.1 MPa and an initial temperature of 293 K.

The curves in Fig. 2b represent the numerically calculated dependence of the pressure wave velocity on the gas volume fraction in water with reactive gas bubbles over the α_{20} = 2–40% range for the measurement segments P4–P5 (Fig. 2a, curve *1*), P5–P6 (curve *2*), and P6–P7 (curve *3*). The pressure wave velocity was determined in the same way as in the experiments: for example, for the P5–P6 segment the distance between the sensors P5 and P6 was divided by the time it took for the wave to travel this distance. The symbols in Fig. 2b represent our experimental data acquired at α_{20} = 2 to 10%.

It is clear from Fig. 2b that, at $2 \le \alpha_{20} \le 6\%$, curve *1* is above curves *2* and *3,* and curves *2* and *3* merge. Therefore, the pressure wave decays in the P4–P5 measurement segment; however, in the P5–P6 and P6–P7 measurement segments, it propagates at a constant velocity. At $\alpha_{20} > 6\%$, curves *2* and *3* diverge: the pressure wave velocity in the P6–P7 segment (curve *3*) is lower than in the P5–P6 segment (curve *2*); i.e., the pressure wave decays monotonically in the P4–P5, P5–P6, and P6–P7 regions.

As in Fig. 1b, the calculated velocity of the steady-state pressure wave in the P5–P6 and P6–P7 segments at $2 \le \alpha_{20} \le 6\%$ decreases with an increasing gas volume fraction. In addition, in our calculations the pressure wave propagates at a Mach number of $M = D/c_0$ = 6.6 and 5.9 at α_{20} = 2 and 6%, respectively; that is, essentially supersonic pressure waves are considered. A comparison between the calculated curves and the experimental data points suggests that, on the whole, the calculations are in satisfactory agreement with the experiment.

Figure 3 presents examples of the calculated time histories of pressure in the cross sections in which the sensors P4, P5, and P6 are placed in the MS (see Fig. 2a; hereafter, cross sections 4, 5, and 6) for an initial gas volume fraction of 6%. Clearly, a wave packet arrives at cross section 4: a stepwise leading shock front with

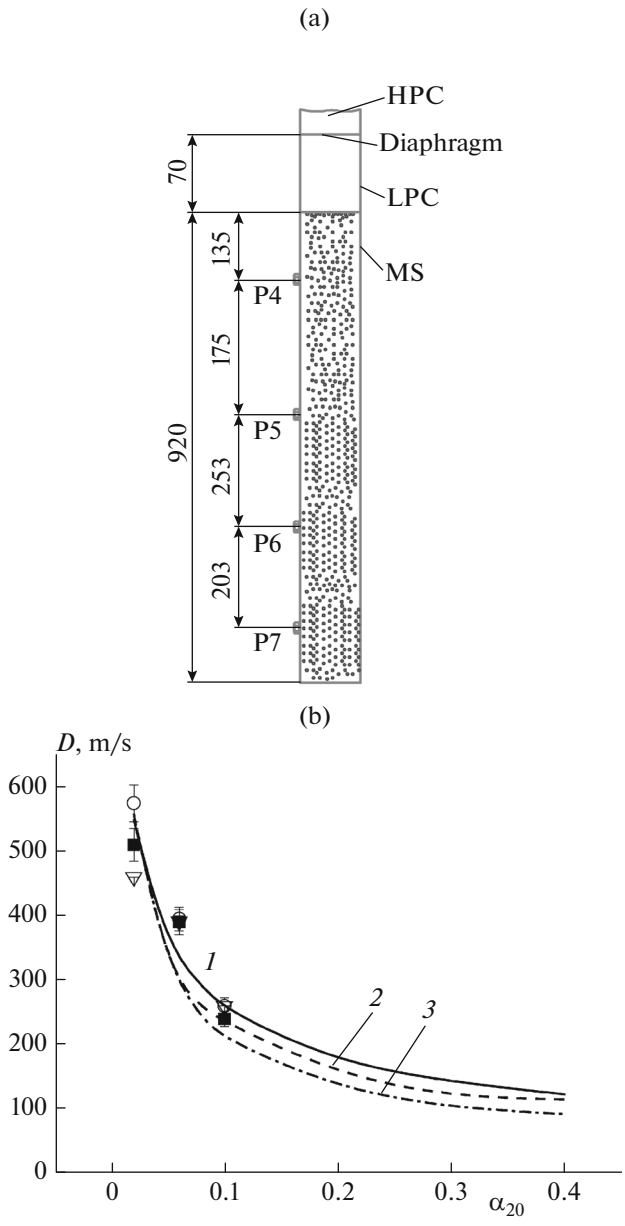

Fig. 2. Comparison of the results of the calculations with our experimental data: (a) experimental setup (dimensions in millimeters); (b) calculated pressure wave velocities as a function of the initial gas volume fraction in water with acetylene–oxygen mixture bubbles (curves) in the (*1*) P4–P5, (*2*) P5–P6, and (*3*) P6–P7 measuring segments and experimental data (symbols) obtained in the same segments: (■) P4–P5, (○) P5–P6, and (▽) P6–P7.

an attached rarefaction wave and a secondary pressure rise is followed by another rarefaction wave and by an SW reflected from the closed end of the HPC. In cross section 5, the stepwise shock front with an attached rarefaction wave is also observed, but there is no secondary pressure rise. The wave packet profile in cross section 6 is precisely the same as in cross section 5, with

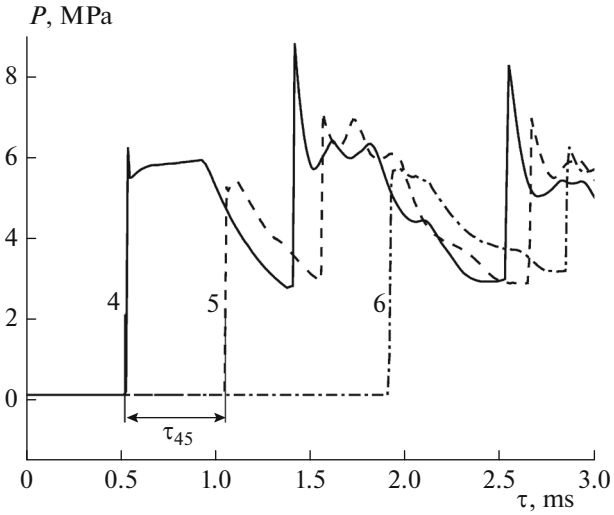

Fig. 3. Examples of calculated time histories of pressure in the cross sections in which the P4–P6 sensors are mounted (cross sections 4–6) for an initial gas volume fraction of 6%: τ, time; τ_{45}, time it takes for the pressure wave front to travel the distance between cross sections 4 and 5; x_{45}, distance between cross sections 4 and 5; $D_{45} = x_{45}/\tau_{45}$ is the pressure wave velocity between cross sections 4 and 5.

the wave packet receding from the reflected SW. The data presented in Figs. 2b and 3 suggest that, in the P5–P6 and P6–P7 segments, as in cross sections 5 and 6, steady-state propagation of a supersonic pressure wave in the bubbly medium takes place.

Figure 4 shows the calculated structure of the supersonic pressure wave at $\alpha_{20} = 6\%$ (Fig. 4a) and 2% (Fig. 4b) at the instant the wave front reaches cross section 5 (1.05 ms in Fig. 3). The width of the acetylene combustion zone in both cases is ~3 mm. Since the velocity of the medium behind the front of the steady-state pressure wave in the moving coordinate system differs only slightly from the velocity of the wave itself (~294 m/s at $\alpha_{20} = 6\%$ and ~556 m/s at $\alpha_{20} = 2\%$), the reaction time is below 15 μs. In other words, in the leading shock front the entire acetylene contained in the gas bubbles burns out very quickly (within <15 μs). The gas temperature in the bubbles increases abruptly to 3900 K (Fig. 4a) and 3500 K (Fig. 4b) and then decreases slowly to ~1200 K (Fig. 4a) and 1500 K (Fig. 4b) in the rarefaction wave. Obviously, the complete burnout of acetylene in the leading shock front of the pressure wave is due to the high temperature developed during the shock compression of the bubbles. The steady-state reaction front with this structure, which propagates at an essentially supersonic speed, should be treated as a detonation-like wave or a "bubble detonation" wave (term suggested by Hasegawa and Fujiwara [5]). Under the conditions accepted in our calculations, bubble detonation was predicted to take place at $2 \le \alpha_{20} \le 6\%$ at a distance of ~300 mm from the exposed surface of the bubbly liquid (cross section 5 in Fig. 2a). At $\alpha_{20} > 6\%$, the calculations led to decaying pressure waves. As in Fig. 1b, in Fig. 2b the calculated upper gas cocnentration limit of bubble detonation is 6%. On the whole, these calculated data are in agreement with the experimental data obtained by Sychev [7], according to which bubble detonation takes place up to $\alpha_{20} = 6\%$. Note that Sychev [7] observed detonation ~2500 mm away from the exposed surface of the bubbly medium, much farther than in our experiments (500–700 mm) and calculations (~300 mm).

Figure 5 presents high-speed camera shots made in one of our experiments at $\alpha_{20} = 2\%$. For obtaining high-contrast images, the videos were recorded using a contre-jour technique. The white dashed lines in Fig. 5 indicate the SW positions determined from bubble deformation onset points in time between two successive video images (separated by a time interval of 25 μs). Some of the images show distinct bright flashes of light resulting from the explosion of separate bubbles.

Figure 5 demonstrates that the SW front travels a distance of $\Delta x \approx 10$ mm as one frame is exposed (exposure time of $\Delta t = 25 \times 10^{-6}$ s). The images show all bubbles that had reacted in the time interval Δt and are within the distance Δx. The bright bubbles, which have undergone explosive conversion, are 10–20 mm behind the SW front; that is, the bubble ignition delay is 25–50 μs and is close to the calculated value, ~15 μs.

It is interesting to follow the variation of the gas volume fraction in the bubble detonation wave versus the variation of the gas volume fraction in the pressure wave propagating in the liquid with chemically inert gas bubbles. Figure 6 illustrates the calculated variation of the gas volume fraction in bubble detonation

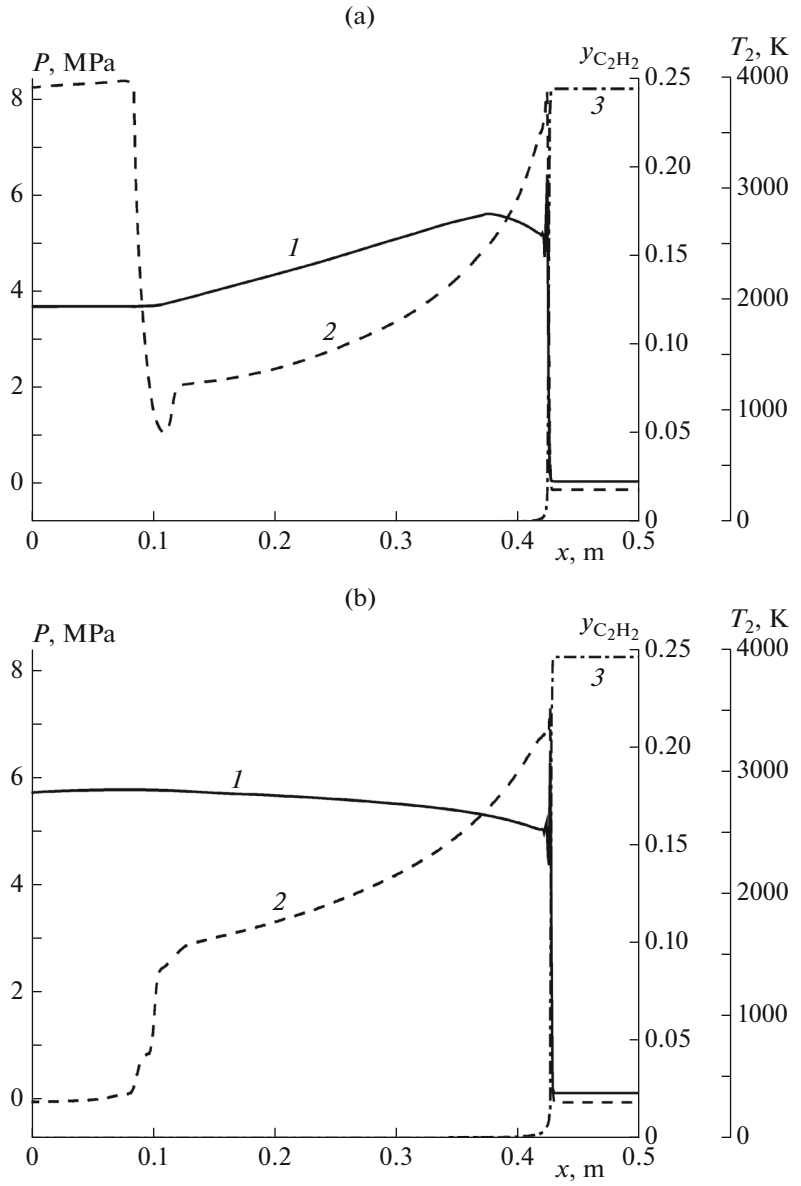

Fig. 4. Structure of the supersonic pressure wave in cross section 5 for initial gas volume fractions of (a) 6 and (b) 2%: (*1*) pressure, (*2*) bubble temperature, and (*3*) acetylene mass fraction in the bubble.

waves at initial gas volume fractions of $\alpha_{20} = 6\%$ (Fig. 6a) and 2% (Fig. 6b), and Fig. 7 plots the same data for pressure waves traveling in water with chemically inert (air) bubbles under the same initial conditions. At the leading front of the bubble detonation wave, the gas volume fraction falls abruptly by a factor of approximately 6 (from 6 to 1% in Fig. 6a and from 2 to 0.3% in Fig. 6b) and then decreases slowly by a factor of about 2 (to 0.6% in Fig. 6a and to 0.17% in Fig. 6b). By contrast, at the SW front depicted in Fig. 7, the gas volume fraction decreases abruptly by a factor of approximately 30–40 (from 6 to 0.2% in Fig. 7a and from 2 to 0.05% in Fig. 7b). Thus, the calculated gas volume fraction behind the leading front of bubble detonation is approximately 3–4 times higher than in the SW propagating in water with air bubbles.

An analysis of the calculated structure of the pressure waves propagating in the bubbly medium at $\alpha_{20} > 6\%$ demonstrates that the combustion zone extends and the maximum temperature of the combustion products decreases gradually with an increasing α_{20}. For example, the calculated width of the acetylene combustion zone is ~5 mm at $\alpha_{20} = 10\%$, ~10 mm at $\alpha_{20} = 20\%$, and ~15 mm at $\alpha_{20} = 30\%$, and the corresponding values of maximum combustion temperature are smaller than in the bubble detonation wave (3900 K) and are 2900, 2600, and 1000 K.

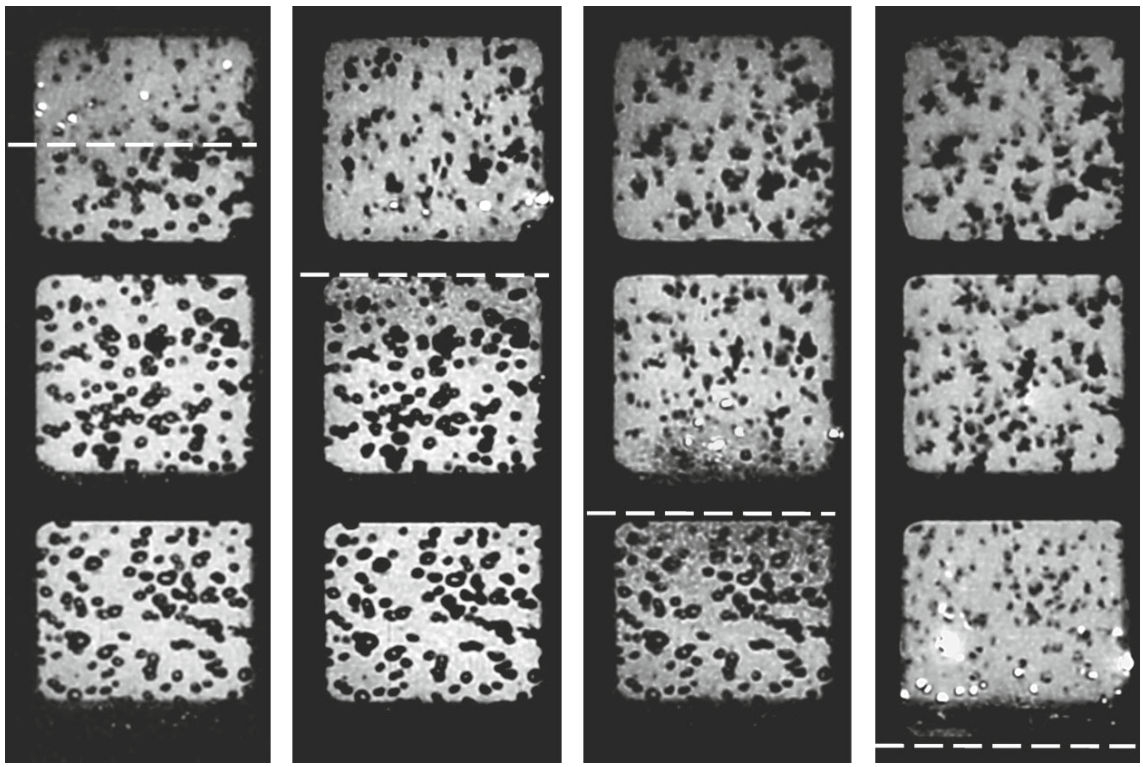

Fig. 5. Video shots of SW propagation in the reactive bubbly medium at $\alpha_{20} = 2\%$ and $P_{0,\,\mathrm{HPC}} = 0.6$ MPa. Time is counted from the ignition point. Frame dimensions, 160 × 448; recording speed, 40000 FPS. The white dashed lines indicate SW front positions.

Momentum Transfer from the Pressure Waves to the Bubbly Medium

Propagating in the bubbly medium at a supersonic speed, the pressure waves set in motion the liquid. This effect can be used to design a hydrojet pulse detonation engine for high-speed vehicles that does not employ a mechanical propulsion device like a propeller, impeller, etc. [1]. This type of engine would eliminate the problem of cavitation destroying mechanical propulsion devices at high flow velocities.

The above calculations make it possible to determine the velocity of the liquid set in motion by the bubble detonation waves (u_1) at $2 \le \alpha_{20} \le 6\%$ and by the decaying pressure waves at $\alpha_{20} > 6\%$. Figure 8 presents the calculated maximum water velocity in the measurement segment P5–P6 (Fig. 2a) as a function of the initial gas volume fraction in water. Clearly, the calculated velocity of the liquid increases with an increasing gas volume fraction, being 12 m/s at $\alpha_{20} = 2\%$ and 40 m/s at $\alpha_{20} = 30\%$. Note that the density of the bubbly liquid decreases as the the gas volume fraction is increased. Therefore, there must be an optimal gas volume fraction maximizing the momentum $(1 - \alpha_{20})\rho_{10}u_1$ transferred from the pressure wave to the bubbly medium. This issue was studied [2–4] theoretically and experimentally for water containing air bubbles.

CONCLUSIONS

Based on two-phase, compressible, viscous, reactive flow equations, we numerically simulated the entry of an SW from a gas into water containing reactive gas (stoichiometric acetylene–oxygen mixture) bubbles uniformly distributed over the volume of the liquid. It was demonstrated that a steady-state supersonic self-sustaining reaction front with complete burnout of the fuel in the leading SW can propagate in this bubbly medium. This reaction front can be treated as a detonation-like front or bubble detonation (term suggested by Hasegawa and Fujiwara [5]). The calculated and measured [7] bubble detonation wave velocities were compared over the initial gas volume fraction range from 2 to 6%: at the boundaries of this range, the detonation velocity was found to be ~400–500 and 200–250 m/s, respectively. The calculated upper gas concentration limit of bubble detonation (5%) is slightly lower than the observed limit (6%). On the whole, the calculated and experimental data are in satisfactory qualitative and quantitative agreement.

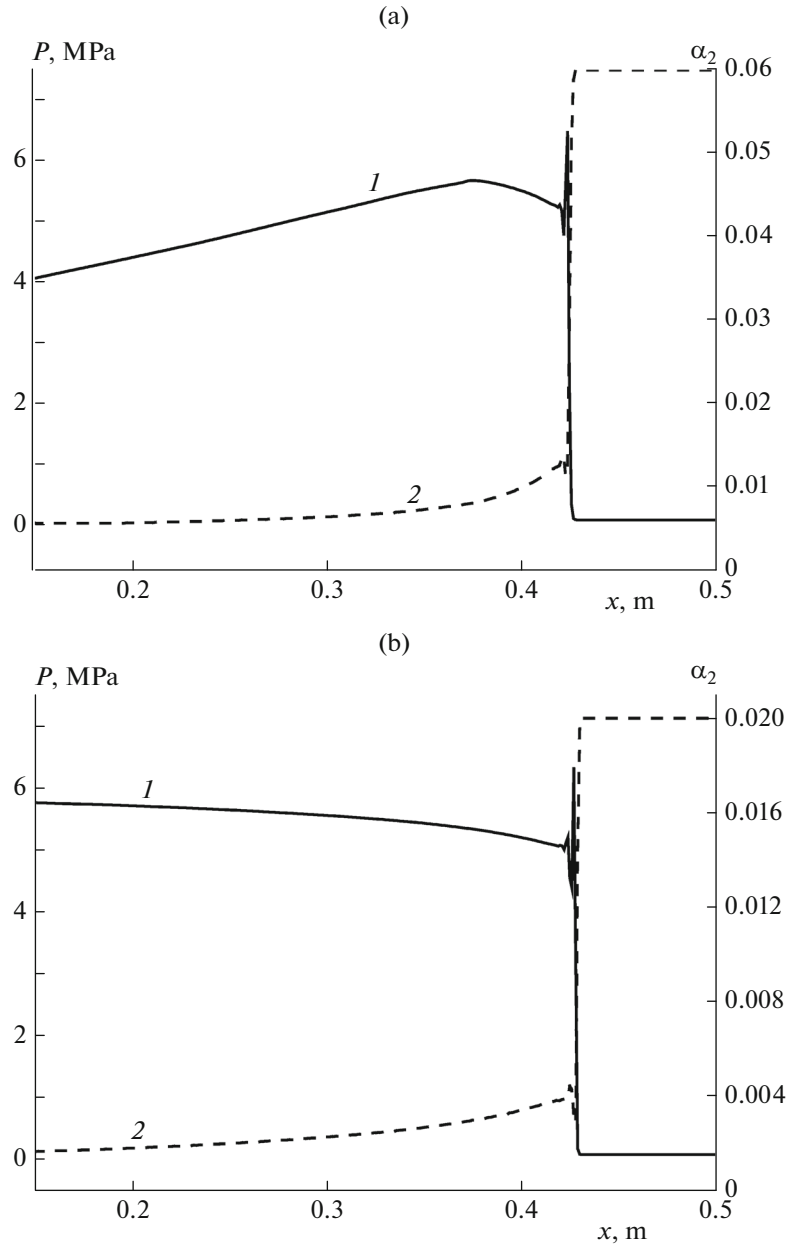

Fig. 6. Structure of the bubble detonation wave in cross section 5 at initial acetylene–oxygen mixture volume fractions of (a) 6 and (b) 2%: (*1*) pressure and (*2*) gas volume fraction.

The specific features of the formation and structure of bubble detonation waves under the conditions of the experiments carried out earlier by the authors were numerically investigated. It was demonstrated that detonation-like pressure waves can form once the SW penetrates to a small depth (~300 mm) into the bubbly medium column. The gas volume fraction in these waves behind the leading front is approximately 3–4 times higher than in the pressure waves propagating in water with air bubbles under the same initial conditions. The calculated velocity of the liquid set in motion behind these waves increases with an increasing gas volume fraction: its value is 12 m/s at $\alpha_{20} = 2\%$ and 40 m/s at $\alpha_{20} = 30\%$. The model suggested here can be used to find the conditions maximizing the efficiency of momentum transfer from the pressure waves to the bubbly medium in promising hydrojet pulse detonation engines.

In forthcoming studies, for refining the structure of the detonation-like waves, we are going to supplement the physical and mathematical model of the phenomenon with the Rayleigh equation for pulsations of a single bubble. Preliminary calculations have demonstrated that, depending on the properties of the bubbly

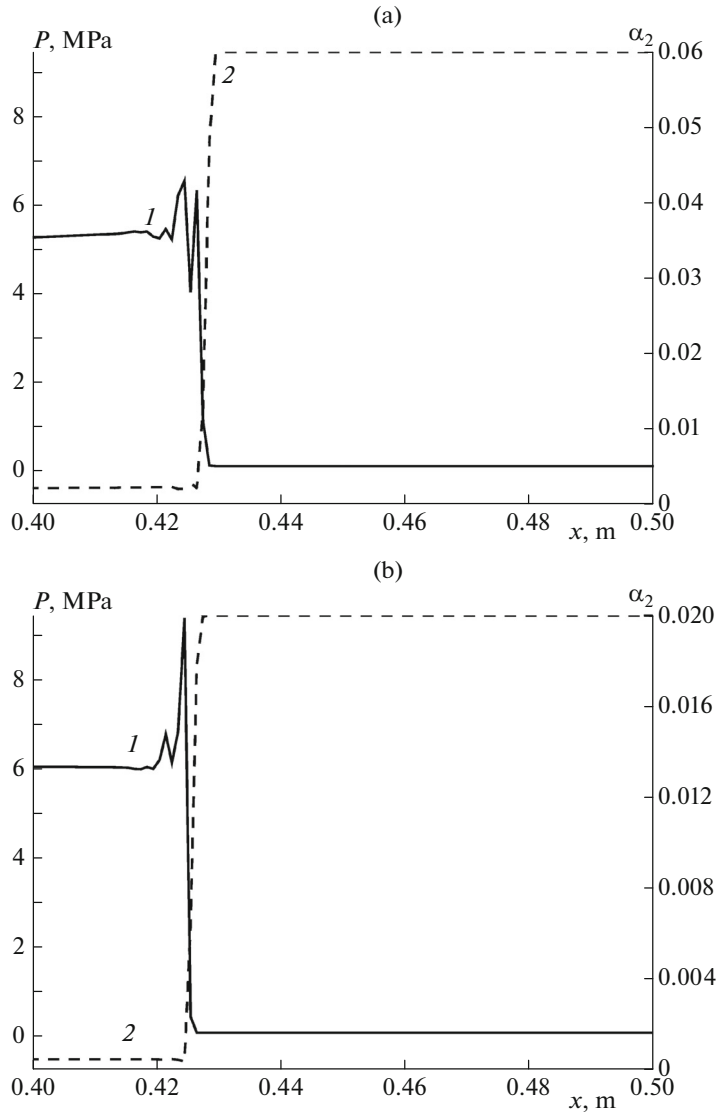

Fig. 7. Structure of the pressure wave in water with air bubbles in cross section 5 at initial gas volume fractions of (a) 6 and (b) 2%: (*1*) pressure and (*2*) gas volume fraction.

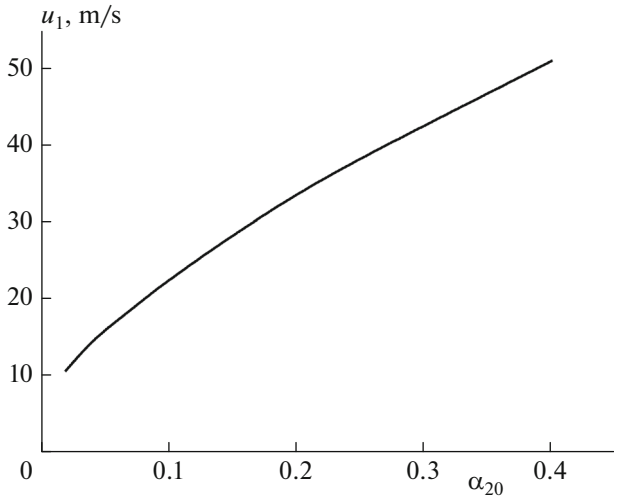

Fig. 8. Calculated maximum liquid velocity as a function of the initial gas volume fraction behind the detonation-like pressure wave front in the P5–P6 measurement segment.

medium, wave packets with different structures, including monotonic, oscillating, solitonic, and multisolitonic structures, can propagate there [19].

ACKNOWLEDGMENTS

This study was supported by the Ministry of Education and Science of the Russian Federation (state contract no. 14.609.21.0001, contract identifier RFMEFI60914X0001).

REFERENCES

1. S. M. Frolov, F. S. Frolov, V. S. Aksenov, and K. A. Avdeev, Request No. PCT/RU2013/001148 (2013). http://www.idgcenter.ru/patentPCT-RU2013-001148.htm
2. K. A. Avdeev, V. S. Aksenov, A. A. Borisov, R. R. Tukhvatullina, S. M. Frolov, and F. S. Frolov, Gorenie i Vzryv (Combustion and Explosion) **8** (2), 57 (2015).
3. K. A. Avdeev, V. S. Aksenov, A. A. Borisov, R. R. Tukhvatullina, S. M. Frolov, and F. S. Frolov, Russ. J. Phys. Chem. B **9**, 363 (2015).
4. K. A. Avdeev, V. S. Aksenov, A. A. Borisov, S. M. Frolov, F. S. Frolov, and I. O. Shamshin, Russ. J. Phys. Chem. B **9**, 895 (2015).
5. T. Hasegawa and T. Fujiwara, in *Proceedings of the 19th International Symposium on Combustion* (Combust. Inst., Pittsburgh, PA, 1982), p. 675.
6. A. I. Sychev, Fiz. Goreniya Vzryva **21** (2), 130 (1985).
7. A. I. Sychev, Fiz. Goreniya Vzryva **21** (3), 103 (1985).
8. A. I. Sychev and A. V. Pinaev, Zh. Prikl. Mekh. Tekh. Fiz., No. 1, 133 (1986).
9. A. V. Pinaev and A. I. Sychev, Fiz. Goreniya Vzryva **23** (6), 76 (1987).
10. A. V. Trotsyuk and P. A. Fomin, Fiz. Goreniya Vzryva **28** (4), 129 (1992).
11. V. Sh. Shagapov and N. K. Vakhitova, Fiz. Goreniya Vzryva, No. 6, 14 (1989).
12. A. V. Pinaev and I. I. Kochetkov, Combust. Explos., Shock Waves **43**, 717 (2007).
13. V. Sh. Shagapov and D. V. Abdrashitov, Fiz. Goreniya Vzryva, No. 6, 89 (1992).
14. S. M. Frolov, V. Ya. Basevich, M. G. Neuhaus, and R. Tatshl, in *Advanced Computation and Analysis of Combustion,* Ed. by G. D. Roy, S. M. Frolov, and P. Givi, (ENAS, Moscow, 1997), p. 537.
15. S. V. Patankar and D. B. Spalding, Int. J. Heat Mass Transfer **15**, 1510 (1972).
16. J. H. Ferziger and M. Peric, *Computational Methods for Fluid Dynamics* (Springer, New York, 1996).
17. P. K. Sweby, SIAM J. Numer. Anal. **21**, 995 (1984). doi doi 10.1137/0721062
18. V. K. Kedrinskii, *Hydrodynamics of Explosion: Models and Experiment* (Sib. Otdel. RAN, Novosibirsk, 2000) [in Russian].
19. S. S. Kutateladze and V. E. Nakoryakov, *Waves and Heat and Mass Transfer in Liquid–Gas Systems* (Nauka, Novosibirsk, 1984) [in Russian].

Translated by D. Zvukov